Aerosol and Air Quality Research, 18: 2005–2013, 2018

ISSN: 1680-8584 print / 2071-1409 online
doi: 10.4209/aaqr.2018.02.0060

Performance of Small Plate and Tube Unipolar Particle Chargers at Low Corona Current

Xiaotong Chen[1,2], Qiaoling Liu[2], Jingkun Jiang[1], Da-Ren Chen[2*]

[1] *State Key Joint Laboratory of Environment Simulation and Pollution Control, School of Environment, Tsinghua University, Beijing 100084, China*
[2] *Particle Laboratory, Department of Mechanical and Nuclear Engineering, School of Engineering, Virginia Commonwealth University, Richmond, VA 23284, USA*

ABSTRACT

Two small chargers, a plate and a tube particle charger, were compared in terms of their performance at low DC-corona current. Both chargers are designed for compact/miniature electrical-mobility-based particle sizers and were operated at a corona current of 0.3 μA for simultaneous low energy consumption and high charging efficiency. A thin wire was utilized in the plate charger for the ion generation via the DC-corona discharge, while a sharp-tipped needle was used in the tube charger. The intrinsic and extrinsic charging efficiencies of particles in various electrical mobility sizes were measured for both chargers at aerosol flow rates of 0.3 and 0.6 L min^{-1}. In general, the plate charger exhibited a lower intrinsic charging efficiency than the tube charger. Also, its extrinsic charging efficiency was slightly higher at 0.3 L min^{-1} than 0.6 L min^{-1} and reached approximately 80% for particles larger than 40 nm. On the other hand, the extrinsic charging efficiency of the tube charger was higher at 0.6 L min^{-1} than 0.3 L min^{-1} for particles larger than 60 nm, with the reverse being true for smaller particles. The extrinsic charge distributions of particles with mobility sizes smaller than 300 nm were also characterized. It was found that a multiple-charge status occurred on particles larger than 20 nm for both chargers. At the same particle size, more charges attached to particles in the tube charger than the plate charger. The birth-and-death charging model was proposed for calculating the extrinsic charge distributions of particles measured in this study. In addition, the Gaussian distribution function was also suggested for best fitting the measured extrinsic charge distributions of particles.

Keyword: Compact/miniature aerosol charger; DC-corona unipolar charger; Small tube charger; Small plate charger; Ultrafine and fine particles.

INTRODUCTION

Recent attention in particle technology, air pollution and public health has been much focused on fine and ultrafine particles due to their potentially adverse effects on public health and the environment (Biswas and Wu, 2005; Patel and Miller, 2009; Martins *et al.*, 2010; Stewart *et al.*, 2010; Paur *et al.*, 2011). To investigate the sources, transport and sinks of submicrometer particles, it is desirable to characterize the size distribution of submicrometer particles in high spatial resolution, especially in the space near the ground. Compact/miniature electrical-mobility-based particle sizers are thus in high demand to achieve the above measurement tasks (Hsiao *et al.*, 2016; Qi and Kulkarni, 2016). An electrical-mobility-based particle sizer is in general composed of three key components: an aerosol charger (i.e., particle charge neutralizer or conditioner), aerosol size classifier (in the operational forms of either electrical precipitator, electrical aerosol classifier, or differential mobility classifier) and particle counter (i.e., either condensation particle counter, electrometer or others.). An aerosol particle charger via either unipolar or bipolar ions is typically used to condition the charge status of sampled particles to a well-defined state. The overall performance of an electrical-mobility-based particle sizer strongly depends on the aerosol charger used in the sizers. For ultrafine particles, unipolar particle chargers typically offer higher charging efficiency than bipolar ones (Chen and Pui, 1999; Intra and Tippayawong, 2011). The sources of ion generation in particle chargers are via the radioactive radiation, soft X-ray photoionization or corona discharge. The rigorous regulation on the usage of radioactive materials and the bulk package of soft-X-ray sources prevent their applications in compact/miniature electrical-mobility-based particle sizers. Corona-based particle

* Corresponding author.
Tel.: (804)828-2828
E-mail address: dchen3@vcu.edu

chargers are typically used in compact/miniature electrical mobility particle sizers.

For small unipolar particle chargers, Qi *et al.* (2008) developed a mini-charger, in which a tungsten needle with a sharp tip was inserted concentrically into a metal tube having a hemispherical and perforated dome at one end. When a high voltage was applied to the needle, the corona discharge occurred at the sharp tip of the needle. An ion-driving voltage was applied in the mini-charger to direct unipolar ions from the corona chamber to the charging zone. The operational current for corona discharge in the mini-charger was set at 2 μA in order to achieve the maximal particle charging efficiency. Although the particle charging efficiency of the mini-charger is high, the status of multiple charges on particles is however severe, particularly for particle sizes greater than 100 nm. A small mixing-type unipolar particle charger (SMUC) was developed by Kimoto *et al.* (2010). A gold needle with a sharp tip was used in this charger to generate unipolar ions. Instead of ion-driving voltage, clean sheath air flow was applied in this small mixing-type charger to drive generated ions into the charging zone and mix with the aerosol stream. Although high charging efficiency of particles was obtained for the small mixing-type charger, the extrinsic charge distribution of particles was not reported in the publication. Chien *et al.* (2011) developed a single-wire corona unipolar charger, in which the corona discharge occurred at the small and near-the-tip segment of a gold wire and clean sheath flow was applied to reduce the deposition of charged particles on the outer wall of the charging chamber. Although the feature of sheath air could reduce the particle loss in aerosol chargers (if properly designed), it was inevitable that the concentration of particles exited from the chargers would be diluted (Marquard *et al.*, 2006a, b). The sheath air would also add the complication to the charger design and operation.

For compact/miniature electrical-mobility-based particle sizers, the configuration and operation of particle chargers should be as simple as possible in order to reduce their production and operational costs. Under the above consideration, sheath flow to reduce the particle loss is not a favorable feature for small particle chargers. A small particle charger is favored to operate at low corona current to reduce the energy consumption and elongate the lifetime of the battery (often served as the power source for compact sizers). Additionally, for a unipolar particle charger, a balance between high charging efficiency and the status of multiple charges on particles should be kept in order to accurately recover the size distribution of particles from the measured electrical mobility distributions. High particle charging efficiency of a unipolar charger typically results in severe multiple-charge status on particles. The severe charge status consequently makes it difficult to accurately inverse the particle size distribution from the electrical mobility distribution measured by an electrical-mobility-based sizer. To minimize the multiple-charge status on particles, particularly for sizes greater than 100 nm, it is thus necessary to evaluate the performance of small unipolar particle chargers under the low corona current condition.

In this study, we evaluated the performance of small plate and tube particle chargers operated at low corona current for compact electrical-mobility-based particle sizers. Both studied chargers were operated at the corona current of 0.3 μA. The corona current is much lower than those applied for unipolar particle chargers reported in the works of Park *et al.* (2007), Qi and Kulkarni (2012), and Intra *et al.* (2017). Our evaluation of charger performance included the charging efficiency (both intrinsic and extrinsic) and extrinsic charge distribution of particles. A birth-and-death model was proposed to calculate the extrinsic charge distributions of particles. The selection of small unipolar chargers for compact/miniature electrical-mobility-based particle sizers of different types was finally concluded according to the experimental finding.

COMPACT PLATE AND TUBE UNIPOLAR CHARGERS

The schematic diagram of the prototype DC-corona-based plate and tube particle chargers are shown in Figs. 1(a) and (b), respectively. The small plate charger was constructed by two thick plates made of metal (Fig. 1(a)). Two stainless steel tubes were hard pressed into two plates as the aerosol inlet and outlet of the charger, respectively. The charging channel with the height of 1.59 mm (0.0625″) was built in the bottom plate. A corona discharge cavity was embedded in the top plate. The zones for particle charging and corona discharge were partitioned by a perforated plate. A tungsten wire in the diameter of 50 μm was installed in the corona cavity. A positive high voltage was applied to the wire to create corona discharge along the wire. A small percentage of generated ions diffused to the particle charging channel and mixed with aerosol stream. The concentration of ions in the charging channel could be tuned by varying the applied high voltage. For simplicity, no sheath flow or ion-driving voltage was featured in the small plate charger. Particle stream was sampled into the charger from the top-left aerosol inlet tube, passed through the charging channel and exited from the bottom-right aerosol outlet tube. The prototype plate charger had the overall size of 59.7 mm × 31.8 mm × 22.2 mm (i.e., 2.35″ × 1.25″ × 0.875″) in length × width × height.

The prototype tube charger inherited the design of mini-charger (Qi *et al.*, 2008). As shown in Fig. 1(b), the tube charger consisted of two metal tubes coaxially aligned. The overall size of small tube charger remained 25.4 mm (1″) in length and 12.7 mm (0.5″) in diameter. The outer tube served as the charger case, which was on the electrical ground. The inner tube was the corona discharge chamber, which was electrically insulated from the outer tube. Instead of a perforated dome in the mini-charger, a perforated disk was designed at the end of the corona tube to reduce the manufacture cost. The particle charging zone was thus defined by the perforated disk of the corona tube and the outer tube. A tungsten needle with a sharp tip was coaxially installed along the axis of the corona tube. A positive high voltage was applied to the needle. The DC corona discharge occurred at the sharp needle tip once the electric field intensity around the tip exceeded the air breakdown strength. An ion-driving voltage was applied on the corona tube. The

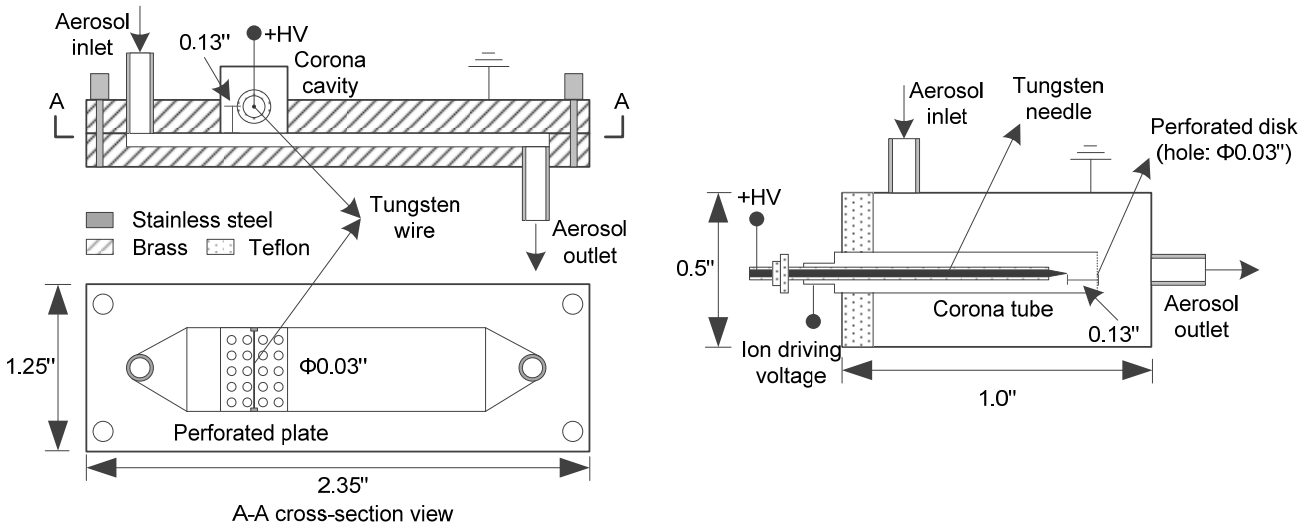

(a) Small plate particle charger (b) Small tube particle charger

Fig. 1. Schematic diagram of prototype DC-corona-based, (a) small plate particle charger and (b) small tube particle charger (units in inches).

weak electric field in the particle charging zone facilitated generated ions moving into the charging zone and stabilized the corona operation at very low current. Particles entered the charger from the aerosol inlet tube installed near the one end of outer tube, moved in the annular space between the corona and outer tubes, reached the charging zone where they mixed with unipolar ions, and finally exited the charger via the aerosol outlet tube installed on the other end of outer tube. The concentration of unipolar ions in the charging zone could be varied by either changing the applied high voltage to the needle and/or ion-driving voltage.

EXPERIMENTAL SETUP FOR CHARGER EVALUATION

The performance evaluation of two studied chargers includes the measurement of the intrinsic and extrinsic charging efficiency, and particle charge distribution. For the measurement of particle charging efficiency, an experimental setup similar to that published in the work of Li and Chen (2011) was used herein. NaCl particles with electrical mobility sizes ranging from 10 to 450 nm were classified either by a Nano-DMA (Model 3085, TSI Inc.) or a long DMA (Model 3081, TSI Inc.). DMA-classified particles were then directed through a Po^{210} neutralizer and an electrostatic precipitator to obtain neutral particles (shown in Fig. 2(a)). The setup to measure the charging efficiency is shown in Fig. 2(b). The method used by Romay and Pui (1992) was applied to measure the intrinsic charging efficiency of test particles. The extrinsic charging efficiency of test particles was evaluated by the method described in the work of Chen and Pui (1999). Eq. (1) calculates the charging efficiencies for particles with different sizes from the measured raw data.

$$\eta_{in} = 1 - \frac{N_1}{N_2}, \quad \eta_{ex} = \frac{N_3 - N_1 / T}{N_4} \tag{1}$$

where η_{in} and η_{ex} are the intrinsic and extrinsic charging efficiency respectively; N_1 and N_2 are the particle number concentration downstream the 2nd electrostatic precipitator (EP) when both the charger and the applied voltage to the 2nd EP are on or off respectively; N_3 is the particle concentration downstream the tested charger when the charger voltage is on; T is the transmission efficiency of neutral particles passing through the 2nd EP; N_4 is the number concentration upstream of the tested charger. Note that, different from the intrinsic charging efficiency of particles, the particle extrinsic charging efficiency takes into consideration of charged particle loss inside the charger.

Fig. 2(c) shows the setup to measure the electrical charge distribution on test particles. A TSI SMPS (scanning mobility particle sizer, with UPCP 3776) without the Kr^{85} neutralizer was used for particles carrying no-greater-than-four elemental charges. For particles with more-than-four elementary charges, a calibrated EP was used instead of an SMPS. A piecewise deconvolution scheme similar to that proposed by Li *et al.* (2006) was used to obtain the charge distributions on particles. Note that the particle charge distributions measured in this part of study should be considered as extrinsic charge distributions of particles, not intrinsic charge distributions of particles.

RESULTS AND DISCUSSION

The intrinsic particle charging efficiency of a unipolar particle charger is primarily affected by the $N_i t$ value (where N_i is the ion concentration and t is the particle residence time in the particle charging zone). The particle residence time in the charging zone could be varied by the aerosol flow rate. For the small plate charger, the ion concentration in the charging zone was controlled via the variation of corona current only. For the small tube particle charger, the ion concentration in the charging channel was tuned by varying either the corona current or ion-driving voltage.

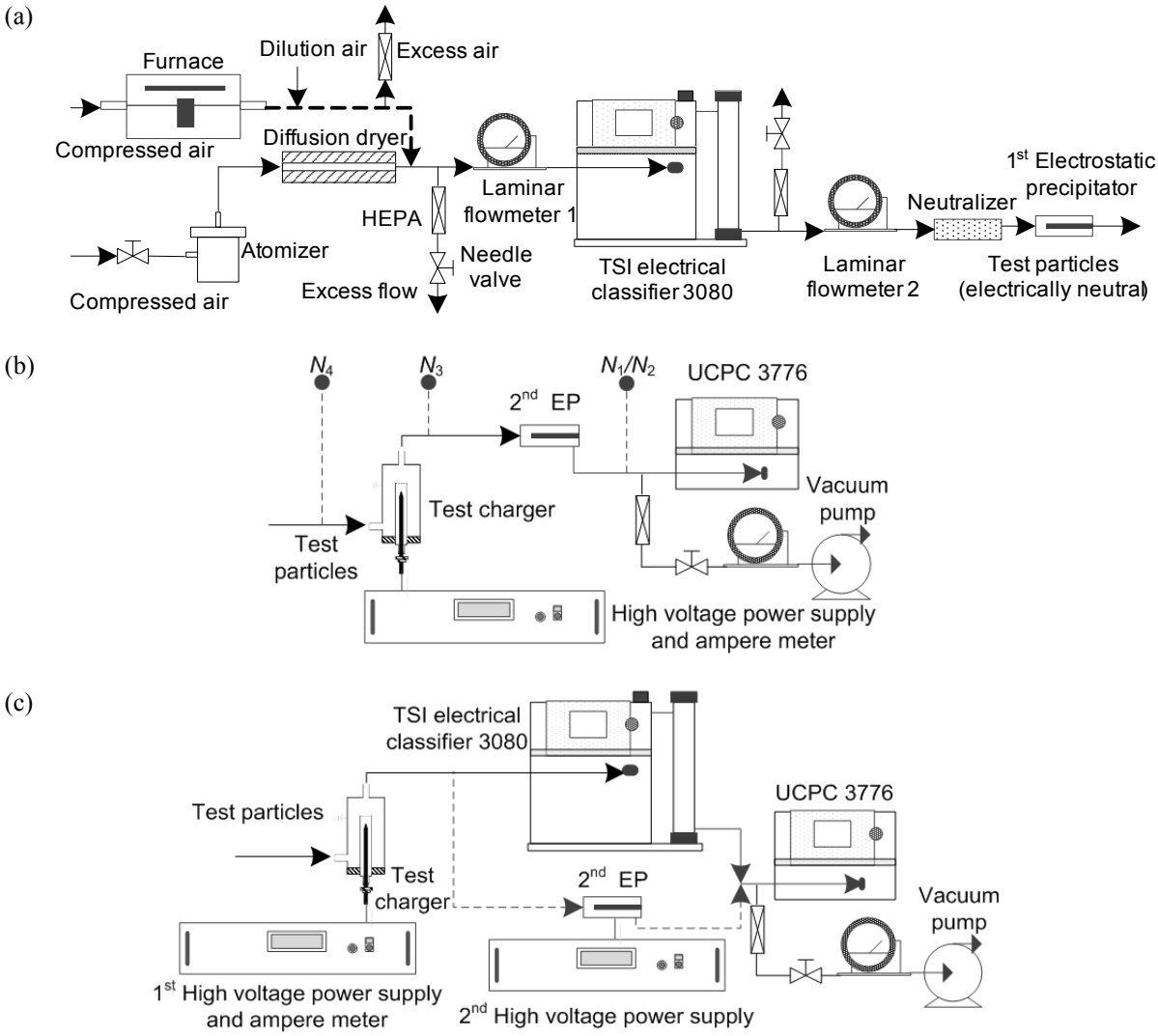

Fig. 2. Experimental setups (a) for the generation of neutral DMA-classified test particles, (b) for the measurement of intrinsic and extrinsic charging efficiency, and (c) for the measurement of extrinsic charge distribution.

For both chargers, the corona current of studied chargers was set at 0.3 μA in this study. It is because 0.3 μA is the lowest corona discharge current achievable in both chargers for their continuous operation while having high charging efficiency. The ion-driving voltage of the small tube charger was 30 V. Two aerosol flow rates of 0.3 and 0.6 L min^{-1}, were selected for evaluating the performance of both chargers. The effects of flow rate and/or ion-driving voltage flow rate on the corona current–voltage curve (i.e., I–V curve) for both chargers were shown in SI (Fig. S1) as the reference. It is found that neither flow rate nor ion-driving voltage has obvious effect on the corona I–V characteristics.

Fig. 3(a) shows the intrinsic charging efficiency of particles in the sizes ranging from 10 nm to 450 nm when studied chargers operated at the above voltage and flow rate conditions. At a given particle size, the intrinsic particle charging efficiency of both chargers increased when the aerosol flow rate decreased. This is due to the increase of particle residence time in the particle charging zone of studied chargers. In general, the small tube charger has a higher intrinsic particle charging efficiency than the small plate charger. This is because of higher ion concentration in the particle charging zone of the small tube charger compared with that of the small plate charger. The best-fitted equations in the format of $\eta = a \times (1 - \exp(-b \times d_p))$ for two studied chargers operated at two aerosol flow rates are also included in Fig. 3(a). The coefficients for each fitted equation are also given in Table S1.

The extrinsic particle charging efficiencies of the studied plate charger and the tube charger at the aerosol flow rates of 0.3 and 0.6 L min^{-1} is shown in Fig. 3(b). Also included in the same figure are the best-fitted equations for measured data sets. The coefficients associated with each equation can be found in Table S1. For the small plate charger, the extrinsic particle charging efficiency at the 0.3 L min^{-1} aerosol flow rate was slightly higher than that at 0.6 L min^{-1} aerosol flow rate. It is because of longer particle residence time at the flow rate of 0.3 L min^{-1}. The extrinsic particle charging efficiency reached a constant of ~80% for particles in sizes larger than 40 nm. For the small tube charger, the

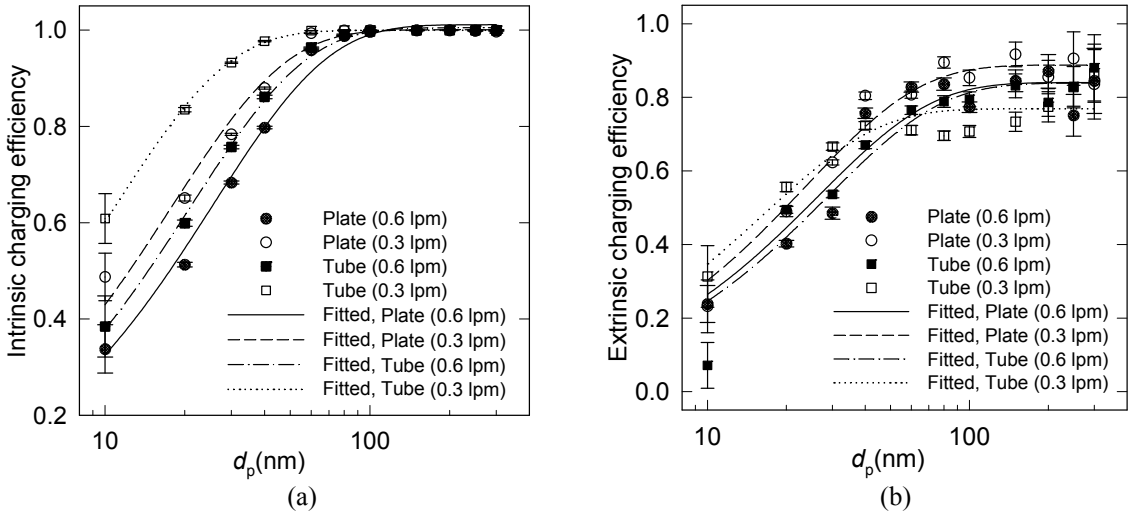

Fig. 3. (a) Intrinsic and (b) extrinsic particle charging efficiencies of small plate and tube particle chargers (operated at the flow rates of 0.3 and 0.6 L min^{-1}) as a function of particle size. Also shown are the fitted curves.

extrinsic charging efficiency at the 0.3 L min^{-1} flow rate was lower than those at the 0.6 L min^{-1} flow rate for particles in sizes greater than 60 nm. This is because large particles carry more electrical charges. Once electrically charged, particles in large sizes were easily lost in the charging zone of the tube charger due to the presence of the weak electrical field and the longer particle residence time at the flow rate of 0.3 L min^{-1} compared with that in the case of 0.6 L min^{-1} flow rate. However, the above observation was reversed for particles with sizes less than 60 nm. This is possibly because of the significant reduction on the intrinsic particle charging efficiency when the small tube charger operated at the 0.6 L min^{-1} flow rate. Compared with the small plate charger, the small tube charger in general had higher intrinsic charging efficiency but comparable extrinsic charging efficiency for particles in the submicrometer sizes when operated at the same aerosol flow rate.

Fig. 4 shows the extrinsic charge distribution of test particles in various electrical mobility sizes for both small plate and tube particle chargers operated at 0.3 and 0.6 L min^{-1}. Particles with sizes of 20, 40, 60, 80, 100, 150, 200, 250 and 300 nm were tested in this experiment. Fig. 4 only shows the extrinsic charge distributions of particles in sizes of 20, 60, 100 and 200 nm for discussion. All the measured extrinsic charge distributions of test particles for two studied chargers are included in Fig. S2 for the reference. For the small plate charger, particles with sizes less than 20 nm are all singly charged. Multiple charges on particles were observed for those with sizes larger than 20 nm. For the 200 nm size, particles carried up to ten elementary charges and had the dominant charge number of 5 and 6 for the 0.6 and 0.3 L min^{-1} flow rates, respectively. For the small tube charger, particles with 200 nm in size had the dominant charge number of 6 and 8 for 0.6 and 0.3 L min^{-1} flow rates, respectively. The measured charge distributions of particles moved towards the high charge number as the particle size increased. Compared to the small plate charger, the small tube charger enabled particles to attach more ions. It is thus concluded that the small tube charger is better applied in the electrical-mobility-based particle sizers with either electrostatic precipitators or electrical aerosol classifiers (EACs) as the size alternators. The small plate charger is suitable for the mobility sizers with differential mobility classifiers as the size classifiers.

For the inversion of particle size distribution based on the data measured by electrical-mobility-based particle sizers, the extrinsic charge distributions of particles at various sizes are required. It is thus useful to have a model capable of calculating the extrinsic charge distributions for particles with sizes other than those tested in the experiment. A simple solution is to fit the extrinsic charge distributions by the birth-and-death particle charging model (Boisdron and Brock, 1970) with the ion-particle combination coefficients estimated by the Fuchs limiting sphere theory (Fuchs, 1963; Hoppel and Frick, 1986). We assumed the mobility and mass of positive ions are 1.15 × 10^{-4} m^2 V^{-1} s^{-1} and 140 relative atomic mass (Hussin *et al.*, 1983) respectively. The $N_i t$ value in the model was obtained by best fitting all the measured extrinsic charge distributions for each studied particle charger operated at each flow rate. $N_i t$ values for the plate charger are 4.16 × 10^{12} s m^{-3} and 6.40 × 10^{12} s m^{-3} at 0.6 and 0.3 L min^{-1} flow rate respectively, and are 5.37 × 10^{12} s m^{-3} and 1.12 × 10^{13} s m^{-3} for the tube charger correspondingly. The comparison of calculated and measured extrinsic charge distributions of particles in various electrical mobility sizes for the studied plate charger and the tube charger operated at 0.3 and 0.6 L min^{-1} aerosol flow rates is shown in Fig. 5. Reasonable agreement between the calculated and measured ones was obtained via the proposed approach above.

The shape of the measured extrinsic charge distributions is similar to a Gaussian distribution, so we used the Gaussian distribution function (i.e., $f = a\exp[-\frac{(q-q_0)^2}{2b^2}]$) to fit the measured particle charge distributions for both studied particle chargers. We assumed the three parameters

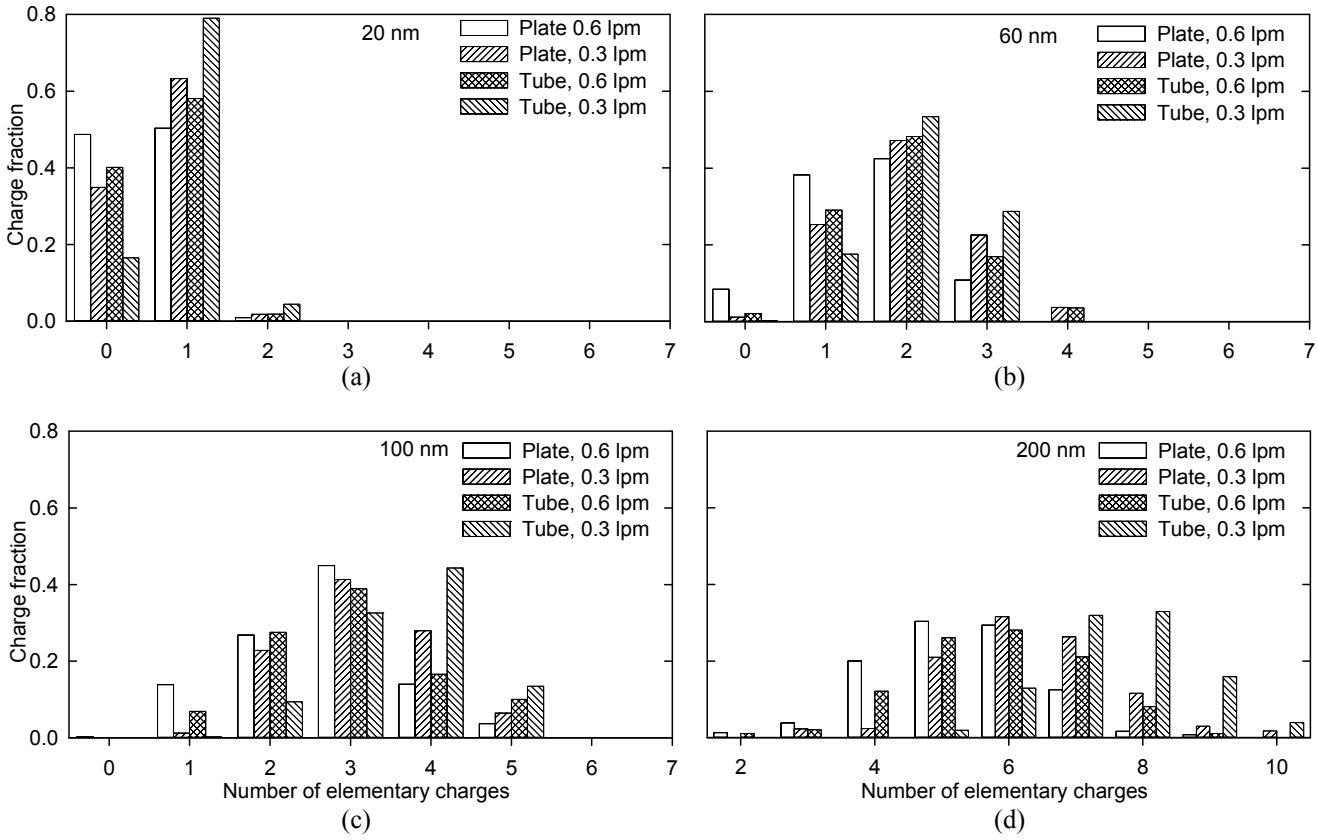

Fig. 4. Measured extrinsic charge distributions of particles for small plate and tube particle chargers: for the particle size of (a) 20 nm, (b) 60 nm, (c) 100 nm and, (d) 200 nm and at 0.3 and 0.6 L min^{-1} flow rates. Note that the measured data for the particle sizes of 40, 80, 100, 150, 200, 250 and 300 are given as the SI.

included in the Gaussian function are functions of the particle Knudsen number (defined as the mean free path of carrier gas molecules to the ratio of particle diameter). The best-fitted Gaussian distribution functions for measured extrinsic particle charge distributions at the flowrate of 0.6 L min^{-1} are given in the following.

$$f(d_p, q) = \left[0.2888 + 0.7432\exp(-1.2796/Kn)\right] \exp\left\{-0.5\left[\frac{q-(1.7608/Kn-0.0442)}{\ln(0.7555/Kn+1.3708)}\right]^2\right\} \quad (2)$$

$$f(d_p, q) = \left[0.2803 + 0.7462\exp(-1.3634/Kn)\right] \exp\left\{-0.5\left[\frac{q-(1.9430/Kn-0.0416)}{\ln(0.7699/Kn+1.4312)}\right]^2\right\} \quad (3)$$

Eqs. (2) and (3) are for the plate and tube chargers, respectively. Kn is the particle Knudsen number in the range of 0.15–4.0; q is the number of elementary charges on particles, which is in the range of 0–14. The Gaussian-fit result is also shown in Fig. 5 as solid curves. Satisfactory agreement between experimental and fitted extrinsic particle charge distributions for two studied particle chargers was also obtained. The fitted Gaussian distribution functions for two studied chargers at the flow rate of 0.3 L min^{-1} are given in Eqs. (S1) and (S2).

CONCLUSION

In this study, we investigated the performance of two compact chargers, a plate and a tube particle charger, operated at low DC-corona-discharge current. Both unipolar chargers are designed for compact/miniature electrical-mobility-based particle sizers. The small plate charger has a particle charging channel built into one thick metal plate and a corona discharge cavity embedded in another. A perforated plate was used to partition the corona cavity and particle charging channel. A Tungsten wire, 50 μm in diameter, was installed in the corona cavity for unipolar ion generation. Generated ions with the same polarity entered the particle charging channel by ion diffusion only. No sheath flow or ion-driving voltage was featured in the small plate charger. The design of the aerosol tube charger used in this study stemmed from that of the mini-charger (Qi at al., 2008) and consists of a corona-discharge tube and an outer tube (i.e., the charger case). Instead of having a perforated dome at the end of the corona tube, like the mini-charger, a perforated disk was implemented in the tube charger. The particle charging zone was established in the space between the perforated disk and the outer tube. A tungsten needle with a sharp tip was inserted along the axis of the corona tube.

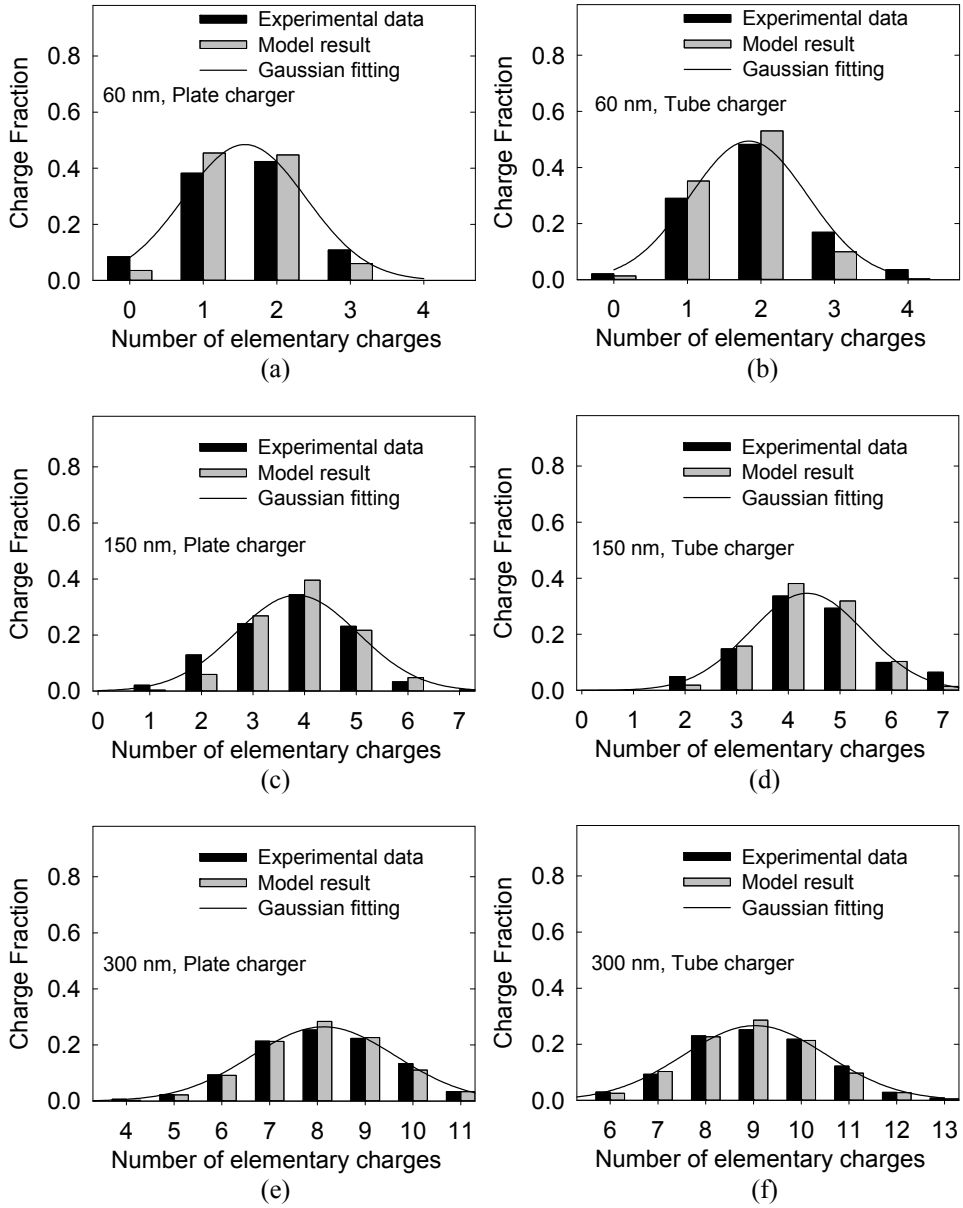

Fig. 5. Comparison of calculated and measured extrinsic charge distributions of test particles for two studied particle chargers at the flowrate of 0.6 L min^{-1}. Also included in the figure are the fitted Gaussian distribution functions. Note that the comparison for all the measured particle sizes is shown in the SI.

The corona discharge occurred at the tip of the needle when a high voltage was applied. Once sampled, particles were transported in the annular space between the corona and outer tubes, entering the charging zone and exiting from the outlet tube installed at the end of the outer tube. An ion-driving voltage of 30 V was also applied between the corona and outer tubes to drive unipolar ions into the particle charging zone and to stabilize the corona operation at low current. Both of the chargers that we studied were operated under their optimal operating conditions, and the corona current was maintained at 0.3 μA for low energy consumption and high charging efficiency.

The intrinsic and extrinsic charging efficiencies of particles with different mobility diameters were measured for both chargers. In general, the plate charger exhibited lower intrinsic charging efficiencies than the tube charger, and its extrinsic charging efficiency was slightly higher at a flow rate of 0.3 L min^{-1} than at a flow rate of 0.6 L min^{-1} due to a longer particle residence time in the particle charging channel for the former flow rate. The extrinsic charging efficiency of the plate charger reached approximately 80% for particles larger than 40 nm. The extrinsic charging efficiency of the tube charger at a flow rate of 0.6 L min^{-1} was higher than at a flow rate of 0.3 L min^{-1} for particles larger than 60 nm because large particles carry more electrical charges, tend to become lost in the charging zone due to the presence of a weak electrical field, and display an increased particle residence time at the latter flow rate. The opposite results were found for particles smaller than 60 nm, which exhibited a reduction in intrinsic charging efficiency at 0.6 L min^{-1}

compared to 0.3 L min^{-1}.

The extrinsic charge distributions of particles with mobility sizes smaller than 300 nm were also characterized at these two flow rates. Multiple charges were observed on particles larger than 20 nm in both chargers. For particles of the same size, fewer electrical charges attached to particles in the plate charger than the tube charger. The birth-and-death charging model with the ion-particle combination coefficients estimated using Fuchs' limiting sphere theory was proposed to calculate the extrinsic particle charge distribution via the variation of N_it values (where N_i is the ion concentration and t is the particle residence time in the charging zone). A reasonable agreement was achieved between the calculated and the measured particle charge distributions for the two chargers. In addition, the Gaussian distribution function was proposed for fitting the measured extrinsic particle charge distributions. Based on the measured distributions, the plate charger is more applicable to electrical-mobility-based sizers with differential mobility classifiers, and the tube charger is more suitable for use in sizers that have either electrostatic precipitators or electrostatic aerosol classifiers.

ACKNOWLEDGMENT

X. Chen would like to thank the Chinese Scholarship Council (CSC) for financial support of the State Scholarship Fund. The authors, Q. Liu and D-R Chen, are grateful for the partial financial support provided by the US EPA STAR program (Grant # 83513201).

COI STATEMENT

D-R Chen, one of the authors, holds the licensed IP, which is similar in name, but unrelated in configuration, to this project.

SUPPLEMENTARY MATERIAL

Supplementary data associated with this article can be found in the online version at http://www.aaqr.org.

REFERENCE

Biswas, P. and Wu, C.Y. (2005). 2005 Critical review: nanoparticles and the environment. *J. Air Waste Manage. Assoc.* 55: 708–746.

Boisdron, Y. and Brock, J.R. (1970). On stochastic nature of acquisition of electrical charge and radioactivity by aerosol particles. *Atmos. Environ.* 4: 35–50.

Chen, D.R. and Pui, D.Y.H. (1999). A high efficiency, high throughput unipolar aerosol charger for nanoparticles. *J. Nanopart. Res.* 1: 115–126.

Chien, C.L., Tsai, C.J., Chen, H.L., Lin, G.Y. and Wu, J.S. (2011). Modeling and validation of nanoparticle charging efficiency of a single-wire corona unipolar charger. *Aerosol Sci. Technol.* 45: 1468–1479.

Fuchs, N.A. (1963). On the stationary charge distribution on aerosol particles in a bipolar ionic atmosphere. *Geofis. Pura Appl.* 56: 185–193.

Hoppel, W.A. and Frick, G.M. (1986). Ion aerosol attachment coefficients and the steady-state charge distribution on aerosols in a bipolar ion environment. *Aerosol Sci. Technol.* 5: 1–21.

Hsiao, T.C., Lee, Y.C., Chen, K.C., Ye, W.C., Sopajaree, K. and Tsai, Y.I. (2016). Experimental comparison of two portable and real-time size distribution analyzers for nano/submicron aerosol measurements. *Aerosol Air Qual. Res.* 16: 919–929.

Hussin, A., Scheibel, H.G., Becker, K.H. and Porstendorfer, J. (1983). Bipolar diffusion charging of aerosol particles - I: Experimental results within the diameter range 4-30 nm. *J. Aerosol Sci.* 14: 671–677.

Intra, P. and Tippayawong, N. (2011). An overview of unipolar charger developments for nanoparticle charging. *Aerosol Air Qual. Res.* 11: 187–209.

Intra, P., Yawootti, A. and Rattanadecho, P. (2017). Corona discharge characteristics and particle losses in a unipolar corona-needle charger obtained through numerical and experimental studies. *J. Electr. Eng. Technol.* 12: 2021–2030.

Kimoto, S., Saiki, K., Kanamaru, M. and Adachi, M. (2010). A small mixing-type unipolar charger (SMUC) for nanoparticles. *Aerosol Sci. Technol.* 44: 872–880.

Li, L. and Chen, D.R. (2011). Performance study of a DC-corona-based particle charger for charge conditioning. *J. Aerosol Sci.* 42: 87–99.

Li, W., Li, L. and Chen, D.R. (2006). Technical note: A new deconvolution scheme for the retrieval of true DMA transfer function from tandem DMA data. *Aerosol Sci. Technol.* 40: 1052–1057.

Marquard, A., Meyer, J. and Kasper, G. (2006a). Characterization of unipolar electrical aerosol chargers - Part I: A review of charger performance criteria. *J. Aerosol Sci.* 37: 1052–1068.

Marquard, A., Meyer, J. and Kasper, G. (2006b). Characterization of unipolar electrical aerosol chargers - Part II: Application of comparison criteria to various types of nanoaerosol charging devices. *J. Aerosol Sci.* 37: 1069–1080.

Martins, L.D., Martins, J.A., Freitas, E.D., Mazzoli, C.R., Goncalves, F.L., Ynoue, R.Y., Hallak, R., Albuquerque, T.T. and Andrade, M.D. (2010). Potential health impact of ultrafine particles under clean and polluted urban atmospheric conditions: A model-based study. *Air Qual. Atmos. Health* 3: 29–39.

Park, D., An, M. and Hwang, J. (2007). Development and performance test of a unipolar diffusion charger for real-time measurements of submicron aerosol particles having a log-normal size distribution. *J. Aerosol Sci.* 38: 420–430.

Patel, M.M. and Miller, R.L. (2009). Air pollution and childhood asthma: Recent advances and future directions. *Curr. Opin. Pediatr.* 21: 235–242.

Paur, H.R., Cassee, F.R., Teeguarden, J., Fissan, H., Diabate, S., Aufderheide, M., Kreyling, W.G., Hänninen, O., Kasper, G., Riediker, M., Rothen-Rutishauser, B. and Schmid, O. (2011). In-vitro cell exposure studies for the assessment of nanoparticle toxicity in the lung—A

dialog between aerosol science and biology. *J. Aerosol Sci.* 42: 668–692.

Qi, C., Chen, D.R. and Greenberg, P. (2008). Performance study of a unipolar aerosol mini-charger for a personal nanoparticle sizer. *J. Aerosol Sci.* 39: 450–459.

Qi, C. and Kulkarni, P. (2012). Unipolar charging based, hand-held mobility spectrometer for aerosol size distribution measurement. *J. Aerosol Sci.* 49: 32–47.

Qi, C. and Kulkarni, P. (2016). Miniature differential mobility analyzer for compact field-portable spectrometers. *Aerosol Sci. Technol.* 50: 1145–1154.

Romay, F.J. and Pui, D.Y.H. (1992). On the combination coefficient of positive-ions with ultrafine neutral particles in the transition and free-molecule regimes. *Aerosol Sci. Technol.* 17: 134–147.

Stewart, J.C., Chalupa, D.C., Devlin, R.B., Frasier, L.M., Huang, L.S., Little, E.L., Lee, S.M., Phipps, R.P., Pietropaoli, A.P., Taubman, M.B., Utell, M.J. and Frampton, M.W. (2010). Vascular effects of ultrafine particles in persons with type 2 diabetes. *Environ. Health Perspect.* 118: 1692–1698.

Received for review, February 19, 2018
Revised, April 13, 2018
Accepted, April 19, 2018